

Accepted Manuscript

Enhancing spectral unmixing by considering the point spread function effect

Qunming Wang, Wenzhong Shi, Peter M. Atkinson

PII: S2211-6753(17)30324-X
DOI: <https://doi.org/10.1016/j.spasta.2018.03.003>
Reference: SPASTA 286

To appear in: *Spatial Statistics*

Received date: 8 December 2017

Accepted date: 13 March 2018

Please cite this article as: Wang Q., Shi W., Atkinson P.M., Enhancing spectral unmixing by considering the point spread function effect. *Spatial Statistics* (2018), <https://doi.org/10.1016/j.spasta.2018.03.003>

This is a PDF file of an unedited manuscript that has been accepted for publication. As a service to our customers we are providing this early version of the manuscript. The manuscript will undergo copyediting, typesetting, and review of the resulting proof before it is published in its final form. Please note that during the production process errors may be discovered which could affect the content, and all legal disclaimers that apply to the journal pertain.



Enhancing spectral unmixing by considering the point spread function effect

Qunming Wang^{a,b,*}, Wenzhong Shi^c, Peter M. Atkinson^{a,d,e,f}

^a Lancaster Environment Centre, Lancaster University, Lancaster LA1 4YQ, UK

^b Centre for Ecology & Hydrology, Lancaster LA1 4YQ, UK

^c Department of Land Surveying and Geo-Informatics, The Hong Kong Polytechnic University, Kowloon, Hong Kong

^d Geography and Environment, University of Southampton, Highfield, Southampton SO17 1BJ, UK

^e School of Geography, Archaeology and Palaeoecology, Queen's University Belfast, BT7 1NN, Northern Ireland, UK

^f State Key Laboratory of Resources and Environmental Information System, Institute of Geographical Sciences and Natural Resources Research, Chinese Academy of Sciences, Beijing 100101, China

*Corresponding author. E-mail: wqm1111@126.com

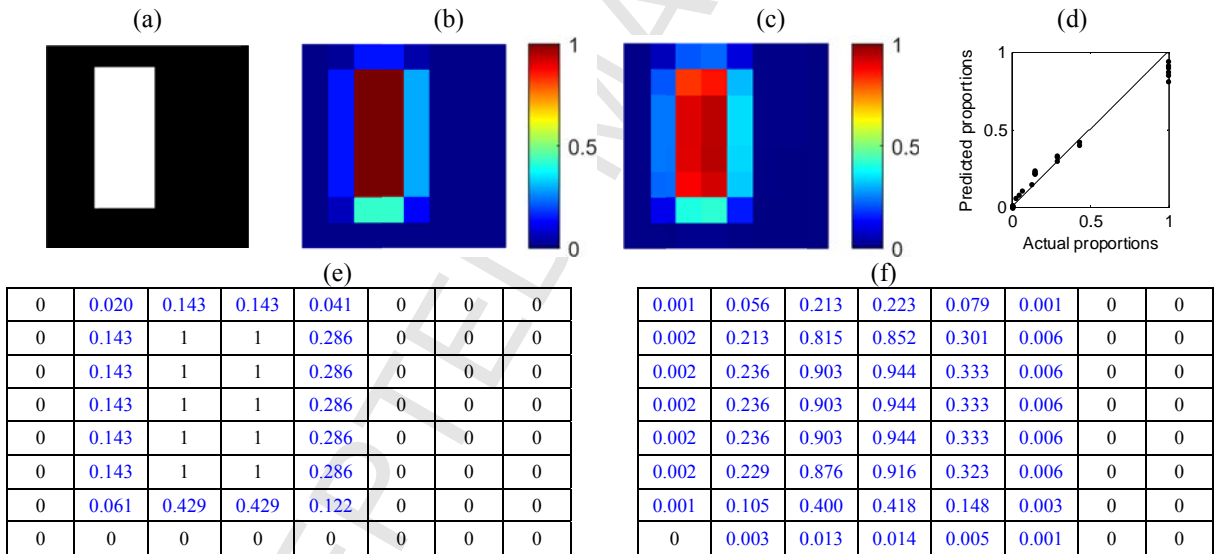
Abstract: The point spread function (PSF) effect exists ubiquitously in real remotely sensed data and such that the observed pixel signal is not only determined by the land cover within its own spatial coverage but also by that within neighboring pixels. The PSF, thus, imposes a fundamental limit on the amount of information captured in remotely sensed images and it introduces great uncertainty in the widely applied, inverse goal of spectral unmixing. Until now, spectral unmixing has erroneously been performed by assuming that the pixel signal is affected only by the land cover within the pixel, that is, ignoring the PSF. In this paper, a new method is proposed to account for the PSF effect within spectral unmixing to produce more accurate predictions of land cover proportions. Based on the mechanism of the PSF effect, the mathematical relation between the coarse proportion and sub-pixel proportions in a local window was deduced. Area-to-point kriging (ATPK) was then proposed to find a solution for the inverse prediction problem of estimating the *sub-pixel* proportions from the original coarse proportions. The *sub-pixel* proportions were finally upscaled using an ideal square wave response to produce the enhanced proportions. The effectiveness of the proposed method was demonstrated using two datasets. The proposed method has great potential for wide application since spectral unmixing is an extremely common approach in remote sensing.

Keywords: Land cover, Spectral unmixing, Soft classification, Point spread function (PSF), Area-to-point-kriging (ATPK).

1. Introduction

Mixed pixels exist unavoidably in remotely sensed images. Mixed pixels cover more than one land cover class such that the observed spectrum is a composite of the individual spectra for the constituent land cover classes (also termed endmembers). Spectral unmixing is the goal of predicting the areal proportions of the land cover classes within mixed pixels and it has been investigated over two decades. It is beyond the scope of this paper to review explicitly the existing methods for spectral unmixing, but several reviews exist (Bioucas-Dias et al., 2012; Quintano et al., 2012). The linear spectral mixture model (LSMM) (Heinz & Chang, 2001; Keshava & Mustard, 2002) underpins the development of most of the existing spectral unmixing methods, with benefits including its clear physical interpretation and mathematical simplicity. LSMM assumes that the spectrum of a mixed pixel is a linear weighted sum of the endmembers.

48 The point spread function (PSF) effect exists ubiquitously in remotely sensed data. It is caused
 49 mainly by the optics of the instrument, the detector and electronics, atmospheric effects, and image
 50 resampling (Huang et al., 2002; Schowengerdt, 1997). The PSF is usually expressed as a 2-D
 51 function (i.e., in both the across-track and along-track directions) (Campagnolo & Montano, 2014;
 52 Radoux et al., 2016). Due to the PSF effect, the signal attributed to a given pixel is a weighted sum
 53 of contributions from not only within the spatial coverage of the pixel, but also that for neighboring
 54 pixels (Townshend et al., 2000; Van der Meer, 2012). Such an effect leads to a fundamental limit
 55 on the amount of information that remote sensing images can contain (Manslow & Nixon, 2002).
 56 Fig. 1 shows an example illustrating the PSF effect on observed coarse proportions. Both visual
 57 and quantitative evaluation shows that when affected by the PSF, the observed coarse proportions
 58 in Fig. 1(c) are obviously different from the actual coarse proportions in Fig. 1(b). The PSF can
 59 brighten dark objects (e.g., increase the actual proportion of zero to a larger value) and darken
 60 bright objects (e.g., decrease the actual proportion of one to a smaller value) (Huang et al., 2002).
 61 In the ideal coarse proportion images, produced with a square wave response, the original boundary
 62 between different land cover classes on the ground always results in a boundary of intermediate
 63 proportions whose width is only one coarse pixel, as shown in Fig. 1(e). Because of the PSF,
 64 however, the width of coarse boundary can be larger than one coarse pixel, shown in Fig. 1(f).
 65 Therefore, the PSF can introduce great uncertainty in proportion estimation based on spectral
 66 unmixing.
 67



70 Fig. 1. An example to illustrate the PSF effect on observed land cover proportions. (a) The simulated 1 m spatial
 71 resolution image of the rectangle target (with target in pure white and background in pure black) on the ground (image
 72 of 56 by 56 pixels). (b) The ideal 7 m coarse spatial resolution proportion image for the target (image of 8 by 8 pixels).
 73 (c) The 7 m coarse spatial resolution proportion image observed using a sensor with a Gaussian PSF (the standard
 74 deviation is half of the coarse pixel size). (d) The relation between the ideal and observed 7 m proportion images in (b)
 75 and (c). (e) and (f) are the corresponding matrices of the proportion images in (b) and (c) (the blue values represent the
 76 boundary cells of the object).
 77

78 It is of great interest to develop methods to consider the PSF effect to produce more accurate
 79 proportions in spectral unmixing. The method needs to consider the impact of spatially neighboring
 80 pixels on the center pixel and eliminate it. It is widely acknowledged that spatial information is
 81 important in spectral unmixing and various methods have been developed on this basis. Shi &

Wang (2014) provided a comprehensive review of existing methods that incorporate spatial information in spectral unmixing. These methods mainly incorporate spatial information in endmember extraction, selection of endmember combinations and abundance estimation. However, very few methods consider the PSF effect from the viewpoint of the physical mechanism. That is, very few studies focus on how the neighboring pixels affect the center coarse pixel based on the PSF effect and consider how to eliminate such an effect. Townshend et al. (2000) and Huang et al. (2002) proposed a deconvolution method to reduce the influence of the PSF in proportion estimation. This method quantifies the contributions from neighbors on the basis of coarse pixel-level information and treats all sub-pixels locations in a coarse neighbor equally. However, different sub-pixel locations in the coarse neighbor have different spatial distances to the center coarse pixel and can have different influences on the center coarse proportion. Therefore, it is necessary to develop methods to consider the impact of neighbors at the sub-pixel scale.

In this paper, we propose a new method to account for the PSF effect in spectral unmixing and produce more accurate proportion predictions. The method predicts the land cover proportions at a finer spatial resolution inversely from the original coarse proportions before predicting the enhanced proportions (i.e., the final predictions at the same coarse spatial resolution with the original proportions, but the PSF effect is reduced). Section 2 first introduces the mechanism of the PSF effect on spectral unmixing and deduces the mathematical relation between the coarse proportions and sub-pixel proportions of both the coarse center pixel and its coarse neighbors. Based on the deduced relation, the area-to-point kriging (ATPK) method is then introduced to predict the sub-pixel proportions from the original coarse proportions. For validation of the method, Section 3 provides and analyzes the experimental results for two datasets. The method is further discussed with several open issues in Section 4. A conclusion is provided in Section 5.

2. Methods

2.1. The effect of the PSF on spectral unmixing

Suppose \mathbf{S}_V is the spectrum of coarse pixel V , $\mathbf{R}(k)$ is the spectrum of class endmember k ($k=1, 2, \dots, K$, where K is the number of land cover classes), and $F_V(k)$ is the proportion of class k within coarse pixel V . Based on the classical linear spectral mixture model, the spectrum of a coarse pixel is a linearly weighted spectra of endmembers, where the weights are class proportions within the coarse pixel:

$$\mathbf{S}_V = \sum_{k=1}^K \mathbf{R}(k)F_V(k). \quad (1)$$

Due to the PSF effect, the spectrum of coarse pixel V can be considered as a convolution of the spectra of sub-pixels

$$\mathbf{S}_V = \mathbf{S}_v * h_v \quad (2)$$

in which \mathbf{S}_v is the spectrum of sub-pixel v , $*$ is the convolution operator and h_v is the PSF. The spectrum of sub-pixel v can be characterized as

$$\mathbf{S}_v = \sum_{k=1}^K \mathbf{R}(k)F_v(k) \quad (3)$$

where $F_v(k)$ is the proportion of class k in sub-pixel v . Substituting Eq. (3) into Eq. (2), we have

$$\mathbf{S}_V = \left[\sum_{k=1}^K \mathbf{R}(k) F_v(k) \right] * h_v = \sum_{k=1}^K \mathbf{R}(k) [F_v(k) * h_v]. \quad (4)$$

124 Comparing Eqs. (1) and (4), we can conclude

$$125 \quad F_v(k) = F_v(k) * h_v. \quad (5)$$

126 This means that the predicted coarse proportion (e.g., based on the classical linear spectral mixture
127 model) within each coarse pixel, $F_v(k)$, is a convolution of the sub-pixel proportions.

128 In theory, the true (i.e., ideal) coarse proportion (denoted as $T_v(k)$) is identified as the average of
129 all sub-pixel class proportions $F_v(k)$ within the center coarse pixel. That is, for $T_v(k)$, the PSF
130 (denoted as h_v') is an ideal square wave filter

$$131 \quad h_v'(i, j) = \begin{cases} \frac{1}{\tau}, & \text{if } (i, j) \in V(i, j) \\ 0, & \text{otherwise} \end{cases}. \quad (6)$$

132 In Eq. (6), τ is the areal ratio between the pixel sizes of V and v , (i, j) is the spatial location of the
133 sub-pixel and $V(i, j)$ is the spatial coverage of the coarse pixel V in which each sub-pixel located
134 at (i, j) falls. Eq. (6) means that based on the square wave filter, only the sub-pixels within the
135 coarse pixel V will affect the coarse pixel and, moreover, all of them will exert the same effect. The
136 relation between $T_v(k)$ and $F_v(k)$ is expressed as

$$137 \quad T_v(k) = F_v(k) * h_v'. \quad (7)$$

138 In reality, the PSF h_v in Eq. (5) is different to the ideal square wave PSF h_v' in Eq. (7) (i.e.,
139 $h_v \neq h_v'$). The spatial coverage of h_v is generally larger than a coarse pixel extent and different
140 sub-pixels may have different effects on the coarse pixel. For example, the PSF is often assumed to
141 be a Gaussian filter (Huang et al., 2002; Townshend et al., 2000; Van der Meer, 2012)

$$142 \quad h_v(i, j) = \begin{cases} \frac{1}{2\pi\sigma^2} \exp\left[-\left(\frac{i^2 + j^2}{2\sigma^2}\right)\right], & \text{if } (i, j) \in V'(i, j) \\ 0, & \text{otherwise} \end{cases} \quad (8)$$

143 where σ is the standard deviation (i.e., the width of the Gaussian PSF) and $V'(i, j)$ is the spatial
144 coverage of the local window centered at coarse pixel V ($V'(i, j)$ is larger than $V(i, j)$ in Eq. (6)).
145 Based on the Gaussian PSF, $F_v(k)$ is actually a convolution of the sub-pixel proportions in the
146 local window centered at the coarse pixel V , rather than being restricted to only the sub-pixel
147 proportions within the coarse pixel V . Moreover, the sub-pixels with different spatial distances to
148 the center coarse pixel will exert different effects on it. Thus, due to the PSF effect, $F_v(k)$ is
149 actually contaminated by the sub-pixels surrounding the coarse pixel V .

150 Evidently, the difference between h_v and h_v' makes the predicted coarse proportion $F_v(k)$
151 different to the ideal coarse proportion $T_v(k)$. The spectral unmixing predictions $F_v(k)$ can,
152 however, be enhanced by considering the PSF effect. To produce more accurate coarse proportions
153 (i.e., predictions that are as close to $T_v(k)$ as possible), the sub-pixel proportions $F_v(k)$ need to be
154 predicted. As seen from Eq. (5), just as $F_v(k)$ is obtained from spectral unmixing, $F_v(k)$ can be
155 predicted inversely once the PSF h_v is known.

2.2. Area-to-point kriging (ATPK) for enhancing the original coarse proportions

The key in the inverse prediction problem of estimating a sub-pixel proportion $F_v(k)$ from coarse proportion $F_v(k)$ is to account for the PSF h_v which introduces the contributions of neighboring pixels to the coarse proportion of center pixel V . This process involves downscaling. ATPK is a powerful choice for downscaling, which can account for the PSF effect explicitly in the scale transformation (Kyriakidis, 2004). In this paper, it is used to downscale the coarse proportions to the finer spatial resolution proportions $F_v(k)$.

Based on ATPK, the sub-pixel proportion is calculated as a linear weighted sum of the neighboring coarse proportions

$$\hat{F}_v(k) = \sum_{i=1}^N \lambda_i F_{V_i}(k), \text{ s.t. } \sum_{i=1}^N \lambda_i = 1 \quad (9)$$

in which λ_i is the weight for the i th coarse neighbor V_i and N is the number of neighbors. The N weights are calculated according to a kriging matrix, where the semivariograms at different spatial resolutions account for the PSF in scale transformation. Details on the kriging matrix and semivariograms can be found in Wang et al. (2015, 2016a).

ATPK has the appealing advantage of honoring the coarse data perfectly. This means that when the ATPK predictions $\hat{F}_v(k)$ are convolved with the PSF h_v , exactly the original coarse proportions $F_v(k)$ are produced (Kyriakidis, 2004)

$$F_v(k) = \hat{F}_v(k) * h_v. \quad (10)$$

By comparing Eqs. (5) and (10), we can consider the ATPK predictions $\hat{F}_v(k)$ as a reliable solution to the inverse prediction problem of estimating the sub-pixel proportions $F_v(k)$.

The final coarse proportion for class k is calculated as a convolution of $\hat{F}_v(k)$ with the ideal square wave filter h_v'

$$\hat{T}_v(k) = \hat{F}_v(k) * h_v'. \quad (11)$$

That is, for each coarse pixel, the final proportion for class k is predicted as the average of $\hat{F}_v(k)$ within it. Fig. 2 describes the process of predicting $T_v(k)$ from the original coarse proportion $F_v(k)$.

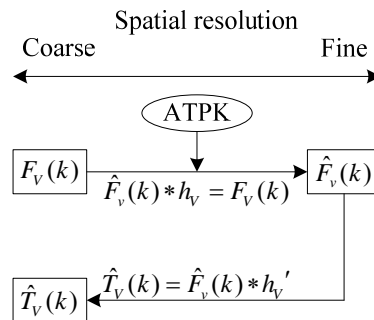


Fig. 2. Flowchart of transforming the original coarse proportion $F_v(k)$ to $T_v(k)$.

188 The implementation of the proposed ATPK-based method that accounts for the PSF in spectral
189 unmixing is not affected by the specific form of PSF and the method is suitable for *any* PSF. Once
190 the PSF is known or predicted, it can be used readily in the method.

191 192 193 **3. Experiments**

194
195 The proposed method for considering the PSF effect in spectral unmixing was demonstrated
196 using two datasets, including a land cover map and a multispectral image. As the estimation of the
197 PSF of sensors remains open and the proposed method is suitable for any PSF, the coarse data
198 (coarse proportions or multispectral image) were synthesized by convolving the available fine
199 spatial resolution land cover map or multispectral image, using the widely acknowledged Gaussian
200 PSF in Eq. (8) (Huang et al., 2002; Townshend et al., 2000; Van der Meer, 2012). The width of the
201 PSF was set to half of the coarse pixel size. The strategy can help to avoid the uncertainty in PSF
202 estimation and concentrate solely on the performance of proportion prediction. Moreover, the
203 coarse proportions are known perfectly and can be used as reference data for evaluation.

204 The root mean square error (RMSE) and correlation coefficient (CC) were used for quantitative
205 evaluation between the proportion predictions and real proportions. To emphasize the increase in
206 accuracy of the predictions of the proposed method over the original ones contaminated by the PSF,
207 an index called the reduction in remaining error (RRE) (Wang et al., 2015) was also used. Details
208 on the calculation of RRE can be referred to Wang et al. (2015).

209 210 *3.1. Experiment on the land cover map*

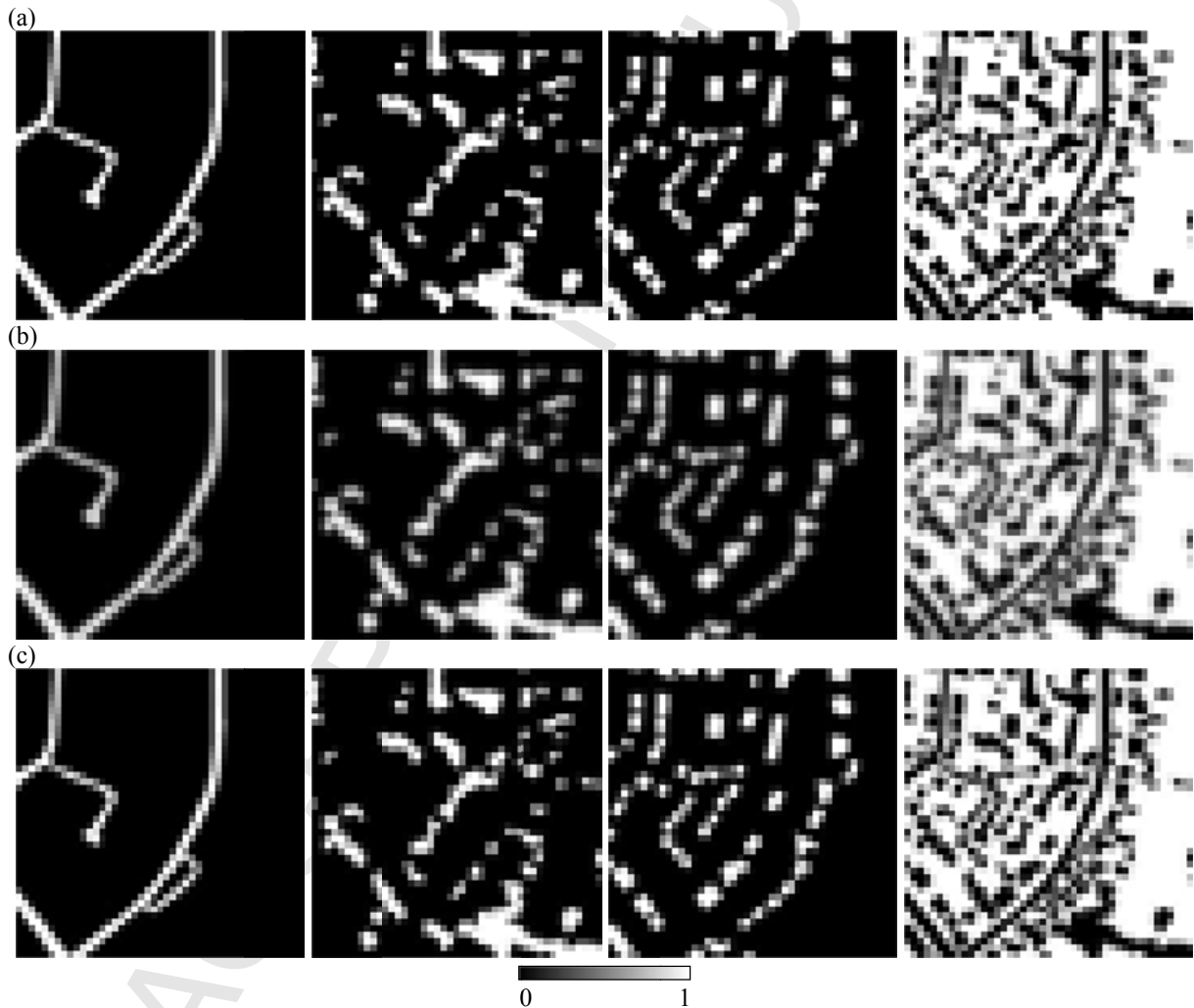
211
212 A land cover map (with a spatial resolution of 0.6 m) covering an area in Bath, UK was used in
213 this experiment, as shown in Fig. 3. The map has a spatial size of 360 by 360 pixels. Four classes
214 were identified in the land cover map, including roads, trees, buildings and grass. The map was
215 degraded by a factor of 8 and a square wave PSF, generating four actual proportion images at a
216 spatial resolution of 4.8 m, as shown Fig. 4(a). Similarly, the four original coarse proportion
217 images produced by spectral unmixing were simulated using a factor of 8 and a Gaussian PSF (the
218 width of the PSF was set to 2.4 m), as shown Fig. 4(b).

219 Fig. 5(a) shows the scatter plots between the actual proportions and original proportions
220 contaminated by the PSF. A visual check of both Figs. 4 and 5 reveals that due to the PSF effect,
221 the original proportions are obviously different from the actual proportions. For example, some
222 actual proportions of 0 are inaccurately predicted as a larger value (for grass, the value can reach
223 0.3, as shown in Fig. 5(a)) and some actual proportions of 1 are inaccurately predicted as a much
224 smaller value (e.g., some of the trees proportions are incorrectly predicted as 0.7, see Fig. 5(a)). Fig.
225 4(c) shows the enhanced proportions produced using the proposed method that considers the PSF
226 effect. Compared with the original proportion images in Fig. 4(b), the enhanced proportion images
227 in Fig. 4(c) are visually closer to the reference in Fig. 4(a). For example, the enhanced proportion
228 images are clearly much brighter than the original proportion images. The scatter-plots between the
229 actual proportions and enhanced proportions accounting for the PSF are shown in Fig. 5(b).
230 Compared with Fig. 5(a), the distribution of points for all four classes in Fig. 5(b) is more compact
231 and closer to the line of $y = x$, suggesting that the enhanced proportions are closer to the actual
232 proportions.
233



Fig. 3. The land cover map used in the first experiment.

234
235
236
237
238



239
240

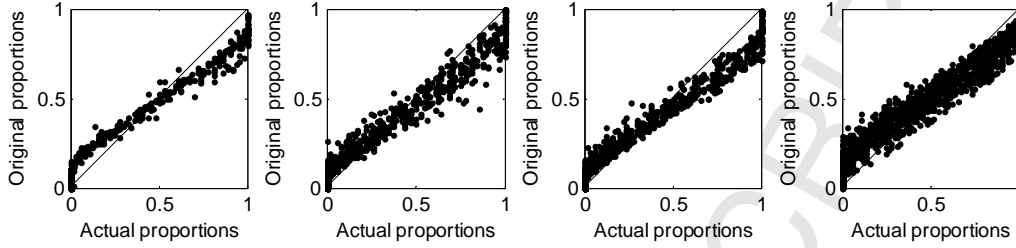
241
242

243
244
245
246
247
248

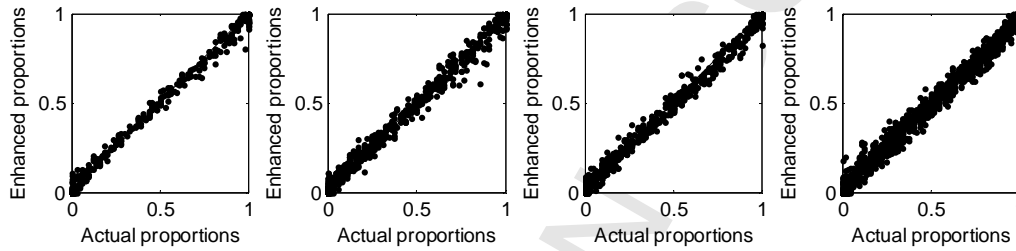
Fig. 4. The proportion images for the land cover map. (a) Reference produced by convolving the the 0.6 m land cover map with an ideal wave square PSF and a degradation factor of 8. (b) Original proportion images produced by convolving the 0.6 m land cover map with a Gaussian PSF and a degradation factor of 8. (c) Enhanced proportions

249 using the proposed method that considers the PSF effect in spectral unmixing. From left to right are the results for
 250 roads, trees, buildings and grass.

251
 252 (a)



253
 254 (b)



255 Fig. 5. (a) Relation between the actual proportions and original proportions in Fig. 4(b). (b) Relation between the actual
 256 proportions and enhanced proportions in Fig. 4(c). From left to right are the results for roads, trees, buildings and grass.
 257
 258

259 Table 1 lists the accuracies of the proportions before and after considering the PSF effect. It is
 260 seen that by considering the PSF effect, the enhanced proportions have larger CCs and smaller
 261 RMSEs than the original proportions. More precisely, the RMSEs decrease by around 0.03, 0.04,
 262 0.04 and 0.06 for roads, trees, buildings and grass, and the RREs are 69.55%, 61.11%, 65.14% and
 263 63.53%. Correspondingly, the RREs for CCs of the four classes are 88.06%, 81.20%, 83.33% and
 264 82.21%, revealing that the errors are greatly reduced by considering the PSF effect.
 265
 266

Table 1 Accuracy of the proportions for the land cover map

		Roads	Trees	Buildings	Grass
RMSE	Original	0.0440	0.0576	0.0591	0.0924
	Enhanced	0.0134	0.0224	0.0206	0.0337
	RRE	69.55%	61.11%	65.14%	63.53%
CC	Original	0.9866	0.9867	0.9844	0.9792
	Enhanced	0.9984	0.9975	0.9974	0.9963
	RRE	88.06%	81.20%	83.33%	82.21%

267
 268 The performance of the proposed method for different PSF width (i.e., 0.25, 0.5, 0.75 and 1) is
 269 shown in Fig. 6. It is clear that the enhanced proportions have consistently larger CCs than the
 270 original proportions for all three cases and all four land cover classes. Moreover, the accuracy gains
 271 become larger when the width increases. For the width of 0.25, the CCs of original and enhanced
 272 proportions are very close (both close to 1, with difference about 0.001), but the difference increase
 273 to be larger than 0.04 for the width of 1. It is worth noting that the accuracies of both original and
 274 enhanced proportions decrease as the width increases.
 275
 276
 277
 278

279

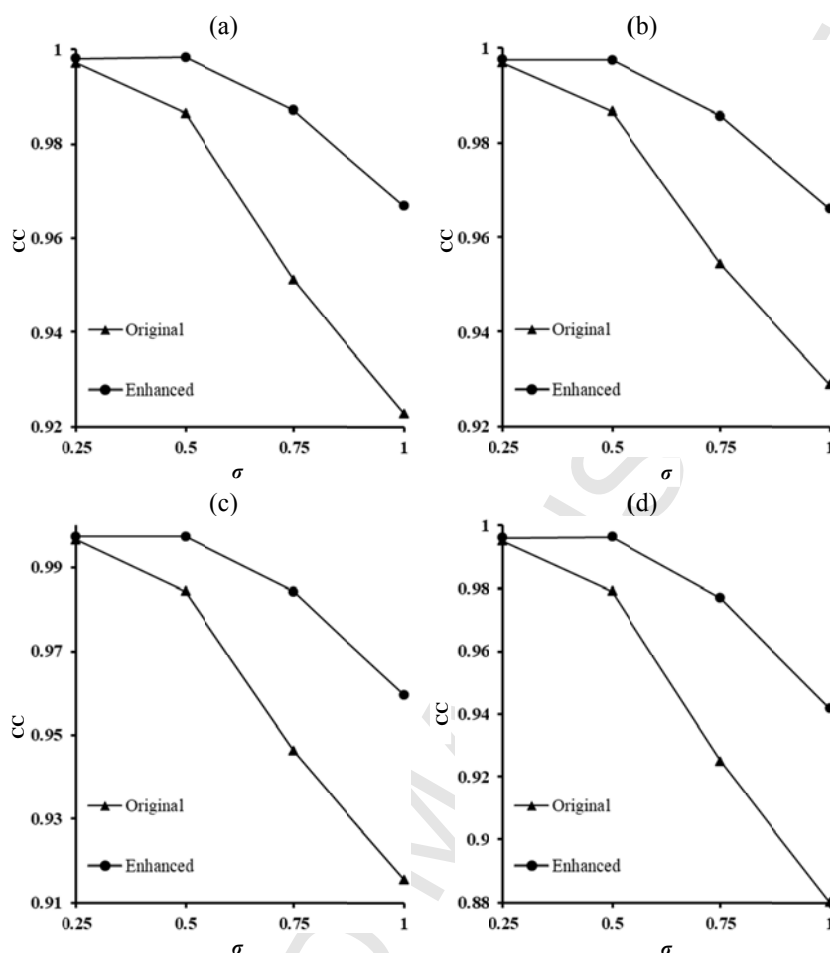
280
281
282283
284

Fig. 6. The CC of the original and enhanced proportions in relation to the width of the Gaussian PSF (in units of coarse pixel). (a)-(d) are results for roads, trees, buildings and grass, respectively.

287

3.2. Experiment on the multispectral image

288

289

290

291

292

293

294

295

296

297

298

299

300

301

302

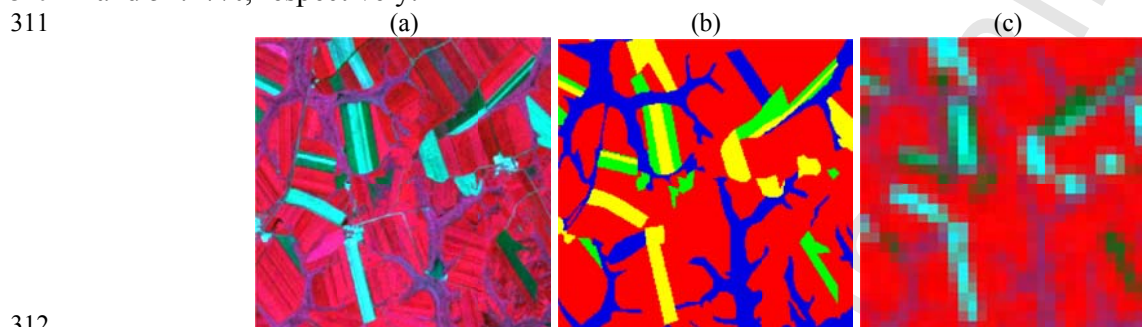
303

304

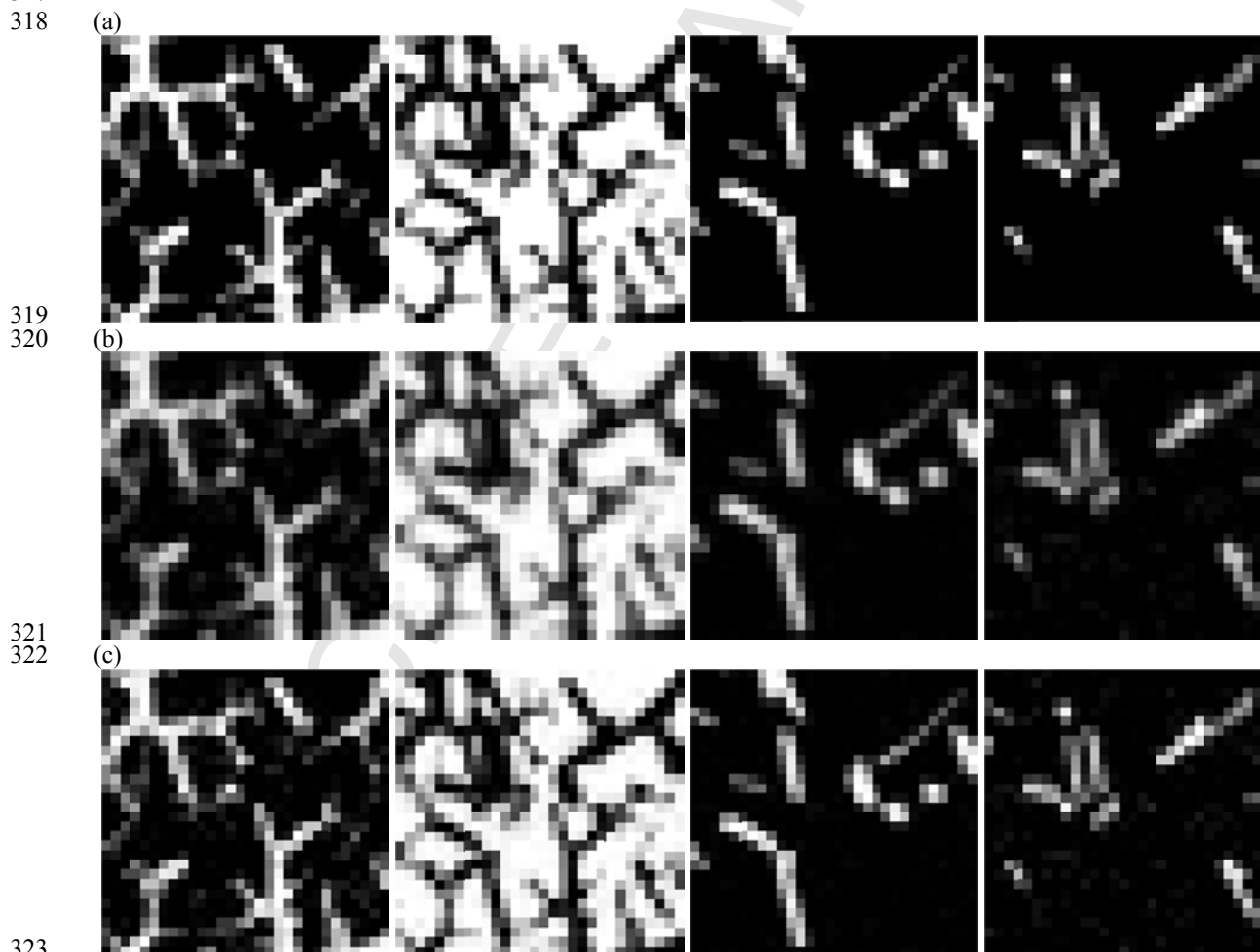
To ensure the perfect reliability of the reference (i.e., actual proportions), a synthesized multispectral image was used in this experiment. Specifically, the image was created from a six-band (bands 1-5 and 7) 30 m Landsat-7 Enhanced Thematic Mapper plus (ETM+) image acquired in August 2001, as shown in Fig. 7(a). The study area has a spatial size of 240 by 240 pixels and covers farmland with four main land cover classes (marked as C1–C4) in the Liaoning Province, China. The corresponding manually digitized land cover map is shown in Fig. 7(b). Referring to the land cover map in Fig. 7(b), the mean and variance of each land cover class in the original six-band 30 m Landsat image were calculated. According to the land cover in Fig. 7(b), a six-band 30 m multispectral image was synthesized based on the random normal distribution and the mean and variance of the classes. Finally, the synthesized 30 m multispectral image was degraded with a factor of 8 and a Gaussian PSF to create a 240 m multispectral image, see Fig. 7(c).

The task of this experiment is to predict the 240 m coarse proportions from the synthesized 240 m multispectral image. The actual 240 m proportions (i.e., reference) were produced by convolving the 30 m land cover map in Fig. 7(b) with an ideal square wave PSF and a degradation factor of 8. Fig. 8 shows the 240 m actual proportions, the original proportions produced without considering

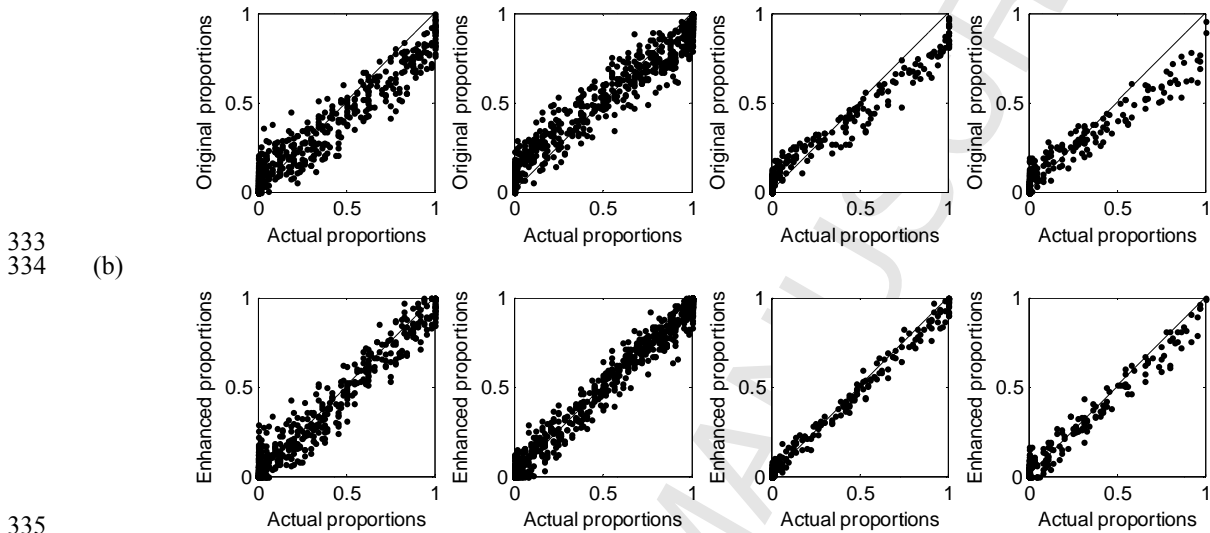
305 the PSF effect and the enhanced proportions produced using the proposed method. It is visually
 306 clear that the enhanced proportions are closer to the reference than the original proportions. This is
 307 also supported by the scatter-plots in Fig. 9. The quantitative assessment is shown in Table 2. By
 308 considering the PSF effect based on the proposed method, the RMSEs for C1–C4 are reduced by
 309 0.03, 0.04, 0.03 and 0.02, and the RREs in terms of CC for C1–C4 are 38.38%, 60.68%, 76.92%
 310 and 52.27%, respectively.



312 Fig. 7. The multispectral image used in the second experiment. (a) Original 30 m multispectral image (bands 432 as
 313 RGB). (b) 30 m land cover map produced by drawing manually from (a) (blue, red, yellow and green represents C1–
 314 C4). (c) 240 m coarse image produced by degrading the synthesized 30 m multispectral image with a Gaussian PSF and
 315 a degradation factor of 8.
 316
 317



324
 325
 326 Fig. 8. The proportion images for the multispectral image. (a) Reference produced by convolving the 30 m land cover
 327 map in Fig. 7(b) with an ideal square wave PSF and a degradation factor of 8. (b) Original proportion images produced
 328 by spectral unmixing of the 240 m coarse multispectral image in Fig. 7(c), without considering the PSF effect. (c)
 329 Enhanced proportions using the proposed method that considers the PSF effect in spectral unmixing. From left to right
 330 are the results for C1–C4.
 331
 332



335
 336 Fig. 9. (a) Relation between the actual proportions and original proportions in Fig. 8(b). (b) Relation between the actual
 337 proportions and enhanced proportions in Fig. 8(c). From left to right are the results for C1–C4. From left to right are the
 338 results for C1–C4.
 339
 340

Table 2 Accuracy of the proportions for the multispectral image

		C1	C2	C3	C4
RMSE	Original	0.0873	0.0950	0.0517	0.0529
	Enhanced	0.0613	0.0540	0.0229	0.0331
	RRE	29.78%	43.16%	55.71%	37.43%
CC	Original	0.9703	0.9766	0.9844	0.9692
	Enhanced	0.9817	0.9908	0.9964	0.9853
	RRE	38.38%	60.68%	76.92%	52.27%

341
 342
 343 **4. Discussion**
 344
 345 After hard land cover classification, spectral unmixing is one of the most common approaches in
 346 remote sensing, and has been applied widely in various domains (Somers et al., 2011), such as
 347 climate change monitoring (Melendez-Pastor et al., 2010), terrestrial ecosystem monitoring (Hestir
 348 et al., 2008), precision agriculture (Pacheco and McNairn, 2010), natural hazard risk assessment
 349 (Eckmann et al., 2010), geological mapping (Bedini, 2009), and urban environment mapping
 350 (Weng et al., 2004). In the last five years, more than 1000 papers were published on spectral
 351 unmixing (indexed in Web of Science). The experimental results reveal that spectral unmixing can
 352 be enhanced by considering the PSF effect through the proposed ATPK-based method. The method
 353 for enhancing the proportions is, thus, expected to have widespread applications in practice. For
 354 example, the global Vegetation Continuous Field (VCF) product has been generated annually from

355 the Moderate Resolution Imaging Spectroradiometer (MODIS) since 2000, which contains the
356 percentage of vegetative cover within each MODIS pixel (DiMiceli et al., 2011). MODIS data have
357 also been used for crop area estimation based on spectral unmixing (Pan et al., 2012). The VCF
358 products and crop area estimation can be potentially enhanced by accounting for the PSF effect.

359 Sub-pixel mapping (Atkinson 1997; Wang et al., 2016b) has been developed for decades, which
360 is a post-processing analysis of spectral unmixing. It creates a thematic map at a finer spatial
361 resolution based on the spectral unmixing predictions as inputs. Specifically, under the proportion
362 coherence constraint and starting with the coarse proportions, sub-pixel mapping divides each
363 mixed pixel into sub-pixels and predicts their land cover class. When the PSF effect is considered
364 in the coarse proportions, more reliable inputs and proportion constraints can be provided for
365 sub-pixel mapping to create more accurate finer spatial resolution land cover maps.

366 According to the relation in Eq. (5), the proposed ATPK-based method can predict sub-pixel
367 proportions (i.e., a by-product) inversely from the coarse proportions. The by-product has a finer
368 spatial resolution than the original proportions and is also expected to have great application value.
369 For example, Gu et al. (2008) produced finer spatial resolution proportion images from input
370 coarse proportion images and the results (e.g., Fig. 10(f) in Gu et al., 2008) showed that aircraft can
371 be observed more clearly from the sub-pixel proportion images. For sub-pixel mapping, the
372 by-product can be hardened to create a finer spatial resolution land cover map, under the proportion
373 coherence constraint from the enhanced coarse proportions. This is also the core idea of the
374 recently developed soft-then-hard sub-pixel mapping algorithm (Wang et al., 2014), which predicts
375 sub-pixel proportion images first and then hardens them to land cover maps. The by-product, along
376 with the enhanced proportions, opens new avenues for future research.

377 In our previous research, the PSF effect was considered directly in the post SPM process (Wang
378 and Atkinson, 2017) to produce more accurate sub-pixel resolution land cover maps. Alternatively,
379 this paper aims to produce more accurate coarse proportions. As discussed above, the coarse
380 proportions have more general applications, including not only in the post SPM process, but also in
381 practical applications such as in large scale crop area and VCF estimation. The by-product of
382 sub-pixel proportions also imposes extra value. It would be interesting to conduct a comparison for
383 SPM predictions based on the method in Wang and Atkinson (2017) and the enhanced coarse
384 proportions produced using the proposed method in this paper.

385 The PSF width (i.e., standard deviation of the Gaussian PSF in this paper) determines how
386 greatly the observed pixel signal is affected by its neighboring pixels. It is a crucial factor affecting
387 the accuracy of spectral unmixing predictions. When the width increases, more neighbors
388 contaminate the center pixel and the uncertainty in predicting the proportions increases as a result,
389 and *vice versa*. Thus, the accuracy of the proportions (either original or enhanced) decreases as the
390 width increases, as reported in Fig. 6. It is worth noting that in Fig. 6, the accuracies of both original
391 and enhanced proportions for the width of 0.25 are nearly the same and both values are close to the
392 ideal value. This reveals that a very narrow PSF (e.g., less than 0.5 pixel) on a discrete grid (i.e.,
393 pixel) has little effect. It should be noted that each sensor has its own PSF width. For example, based
394 on the assumption of the Gaussian PSF, Radoux et al. (2016) found that the width for the Landsat 8
395 red band is 0.72 pixel and ranges from 0.71 to 0.94 pixel for the Sentinel-2 bands. The consistently
396 greater accuracy of the proposed method for different widths suggests its great application value
397 for different sensors.

398 In this paper, a Gaussian PSF was assumed for convenience in the experimental validation. It
399 should be noted that the PSF may not be the Gaussian filter in reality, especially for sensors with a
400 scanning mirror which will ensure that the shape has a directional component (Tan et al., 2006).
401 However, this paper aims to find a solution to account for the PSF effect to enhance spectral

402 unmixing predictions. We did not focus on the specific form of the PSF (e.g., specific form of the
403 function and related parameters), as the proposed method is suitable for any PSF. In practice, once
404 the PSF is available, it can be used readily in the proposed ATPK-based method.

405 It is assumed that the endmembers are scale-free and that the same endmembers can be
406 considered for the coarse and fine spatial resolution spectra in Eqs. (1) and (3). This assumption is
407 more reliable when the landscapes are homogeneous or the intra-class spectra variation is small,
408 such that slight differences exist between the endmembers at different spatial resolutions. However,
409 intra-class spectral variation is a common problem in spectral unmixing that remains open
410 (Drumetz et al., 2016; Somers et al., 2011). It would be worthwhile to investigate the relation
411 between the endmembers at different spatial resolutions, or to consider endmember extraction in a
412 local window and the use of multiple endmembers to characterize each land cover class.

413 The proposed ATPK-based method is shown to be effective in considering the PSF effect, based
414 on the assumption that the ATPK predictions $\hat{F}_v(k)$ are a reliable solution to the inverse prediction
415 problem of estimating sub-pixel proportion $F_v(k)$ from $F_v(k)$. However, this inverse prediction
416 problem is ill-posed, and multiple solutions may meet the coherence constraint in Eq. (10). In
417 future research, it would be interesting to design an appropriate model to incorporate additional
418 information (e.g., prior spatial structure information for each land cover class at the fine spatial
419 resolution) into the ATPK method to reduce the solution space and produce more reliable sub-pixel
420 proportions.

421

422

423 5. Conclusion

424

425 A new method was proposed for considering the PSF in spectral unmixing and increasing the
426 accuracy of land cover proportion predictions. Based on the ubiquitous existence of the PSF effect
427 in real remotely sensed images, spectral unmixing predictions are made as a convolution of the
428 sub-pixel proportions of both the coarse center pixel and coarse neighbors. ATPK is proposed to
429 predict the sub-pixel proportions inversely from the coarse proportions and the sub-pixel
430 proportions are then convolved with the ideal square wave PSF to produce the final predictions.
431 The experimental results on two datasets suggest that the proposed method provides a satisfactory
432 solution for reducing the PSF effect in spectral unmixing.

433

434

435 Acknowledgment

436

437 This work was supported in part by the Research Grants Council of Hong Kong under Grant
438 PolyU 15223015 and in part by the National Natural Science Foundation of China under Grant
439 41331175.

440

441

442 References

443

444 Atkinson, P. M. (1997). Mapping sub-pixel boundaries from remotely sensed images. *Innov. GIS*
445 4, 166–180.

446 Bedini, E., van der Meer, F., van Ruitenbeek, F. (2009). Use of HyMap imaging spectrometer data
447 to map mineralogy in the Rodalquilar caldera, southeast Spain. *International Journal of*
448 *Remote Sensing*, 30, 327–348.

- 449 Bioucas-Dias, J. M., Plaza, A., Dobigeon, N., Parente, M., Du, Q., Gader, P., Chanussot, J. (2012).
450 Hyperspectral unmixing overview: Geometrical, statistical and sparse regression-based
451 approaches. *IEEE Journal of Selected Topics in Applied Earth Observations and Remote*
452 *Sensing*, 5, 354–379.
- 453 Campagnolo, M. L., & Montano, E. L. (2014). Estimation of effective resolution for daily MODIS
454 gridded surface reflectance products. *IEEE Transactions on Geoscience and Remote Sensing*,
455 52, 5622–5632.
- 456 DiMiceli, C., Carroll, M., Sohlberg, R., et al. (2011). Annual global automated MODIS vegetation
457 continuous fields (MOD44B) at 250 m spatial resolution for data years beginning day 65,
458 2000-2010, collection 5 percent tree cover. USA: University of Maryland, College Park, MD.
- 459 Drumetz, L., Chanussot, J., Jutten, C., 2016. Variability of the endmembers in spectral unmixing:
460 recent advances. *8th Workshop on Hyperspectral Image and Signal Processing: Evolution in*
461 *Remote Sensing (WHISPERS 2016)*, Los Angeles, United States.
- 462 Eckmann, T. C., Still, C. J., Roberts, D.A., Michaelsen, J. C. (2010). Variations in subpixel fire
463 properties with season and land cover in Southern Africa. *Earth Interactions*, 14(6).
- 464 Gu, Y., Zhang, Y., Zhang, J. (2008). Integration of spatial–spectral information for resolution
465 enhancement in hyperspectral images. *IEEE Transactions on Geoscience and Remote Sensing*,
466 46, 1347–1358.
- 467 Heinz, D. C., Chang, C. I. (2001). Fully constrained least squares linear spectral mixture analysis
468 method for material quantification in hyperspectral imagery. *IEEE Transactions on*
469 *Geoscience and Remote Sensing*, 39, 529–545.
- 470 Hestir, E. L., Khanna, S., Andrew, M. E., Santos, M. J., Viers, J. H., Greenberg, J. A., et al. (2008).
471 Identification of invasive vegetation using hyperspectral remote sensing in the California Delta
472 ecosystem. *Remote Sensing of Environment*, 112, 4034–4047.
- 473 Huang, C., Townshend, R.G., Liang, S., Kalluri, S. N. V., DeFries, R. S. (2002). Impact of sensor's
474 point spread function on land cover characterization: assessment and deconvolution. *Remote*
475 *Sensing of Environment*, 80, 203–212.
- 476 Keshava, N., Mustard, J. F. (2002). Spectral unmixing. *IEEE Signal Processing Magazine*, 19, 44–
477 57.
- 478 Kyriakidis, P. C. (2004). A geostatistical framework for area-to-point spatial interpolation.
479 *Geographical Analysis*, 36, 259–289.
- 480 Manslow J. F., & Nixon, M. S. (2002). On the ambiguity induced by a remote sensor's PSF. In
481 *Uncertainty in Remote Sensing and GIS*, 37–57.
- 482 Melendez-Pastor, I., Navarro-Pedreno, J., Gomez, I., Koch, M. (2010). Detecting drought induced
483 environmental changes in a Mediterranean wetland by remote sensing. *Applied Geography*, 30,
484 254–262.
- 485 Pacheco, A., McNairn, H. (2010). Evaluating multispectral remote sensing and spectral unmixing
486 analysis for crop residue mapping. *Remote Sensing of Environment*, 114, 2219–2228.
- 487 Pan, Y., Li, L., Zhang, J., Liang, S., Zhu, X., Sulla-Menashe, D., 2012. Winter wheat area
488 estimation from MODIS-EVI time series data using the Crop Proportion Phenology Index.
489 *Remote Sensing of Environment*, 119, 232–242.
- 490 Quintano, C., Fernandez-Manso, A., Shimabukuro, Y., 2012. Spectral unmixing. *International*
491 *Journal of Remote Sensing*, 33, 5307–5340.
- 492 Radoux, J., Chome, G., Jacques, D. C., Waldner, F., Bellemans, N., Matton, N., Lamarche, C.,
493 Andrimont, R., Defourny, P. (2016). Sentinel-2's potential for sub-pixel landscape feature
494 detection. *Remote Sensing*, 8, 488.

- 495 Schowengerdt, R. A. (1997). *Remote sensing: models and methods for image processing*. San
496 Diego: Academic Press.
- 497 Shi, C., Wang, L., 2014. Incorporating spatial information in spectral unmixing: A review. *Remote*
498 *Sensing of Environment*, 149, 70–87.
- 499 Somers, B., Asner, G. P., Tits, L., Coppin, P. (2011). Endmember variability in Spectral Mixture
500 Analysis: A review. *Remote Sensing of Environment*, 115, 1603–1616.
- 501 Tan, B., Woodcock, C. E., Hu, J., Zhang, P., Ozdogan, M., Huang, D., Yang, W., Knyazikhin, Y.,
502 Myneni, R. B. (2006). The impact of gridding artifacts on the local spatial properties of MODIS
503 data: Implications for validation, compositing, and band-to-band registration across resolutions.
504 *Remote Sensing of Environment*, 105, 98–114.
- 505 Townshend, R. G., Huang, C., Kalluri, S. N. V., Defries, R. S., Liang, S. (2000). Beware of
506 per-pixel characterization of land cover. *International Journal of Remote Sensing*, 21, 839–
507 843.
- 508 Van der Meer, F. D. (2012). Remote-sensing image analysis and geostatistics. *International*
509 *Journal of Remote Sensing*, vol. 33, no. 18, pp. 5644–5676, 2012.
- 510 Wang, Q., Shi, W., Wang, L. (2014). Allocating classes for soft-then-hard subpixel mapping
511 algorithms in units of class. *IEEE Transactions on Geoscience and Remote Sensing*, 52, 2940–
512 2959.
- 513 Wang, Q., Shi, W., Atkinson, P. M., Zhao, Y. (2015). Downscaling MODIS images with
514 area-to-point regression kriging. *Remote Sensing of Environment*, 166, 191–204.
- 515 Wang, Q., Shi, W., Atkinson, P. M. (2016a). Area-to-point regression kriging for pan-sharpening.
516 *ISPRS Journal of Photogrammetry and Remote Sensing*, 114, 151–165.
- 517 Wang, Q., Shi, W., Atkinson, P. M. (2016b). Spatial-temporal sub-pixel mapping of time-series
518 images. *IEEE Transactions on Geoscience and Remote Sensing*, 54, 5397–5411.
- 519 Wang, Q., Atkinson, P. M. (2017). The effect of the point spread function on sub-pixel mapping.
520 *Remote Sensing of Environment*, 193, 127–137.
- 521 Weng, Q. H., Lu, D. S., Schubring, J. (2004). Estimation of land surface temperature-vegetation
522 abundance relationship for urban heat island studies. *Remote Sensing of Environment*, 89,
523 467–483.
- 524 Wenny, B. N., Helder, D., Hong, J., Leigh, L., Thome, K. J., Reuter, D. (2015). Pre- and
525 post-launch spatial quality of the Landsat 8 Thermal Infrared Sensor. *Remote Sensing*, 7, 1962–
526 1980.